2022 21st International Conference on Micro and Nanotechnology for Power Generation and Energy Conversion Applications (PowerMEMS) | 978-1-6654-9306-2/22/$31.00 ©2022 IEEE | DOI: 10.1109/PowerMEMS56853.2022.10007608

ULTRA-LOW POWER GAS SENSOR BASED ON A 3D ARRAY OF NANOGAPS

Farhan Sadik Sium[1], Shakir-ul Haque Khan[1], Seungbeom Noh[1], Rana Dalapati[2], Ling Zang[2], Carlos Mastrangelo[1], and Hanseup Kim[1]
Electrical and Computer Engineering[1], and Materials Science and Engineering[2],
University of Utah, USA

ABSTRACT

This paper reports the achievement of ultra-low-power operation under 10 nW by utilizing a wake-up function through a 3D-nanogap (~5 nm) structure consisting of 16×16×2 and 25×25×2 isolated conducting plate arrays. This 3D-nanogap structure improves the previous 2D-one by establishing multiple parallel possible conduction paths in 3D. It thus results in lower operation voltage down to a level (<3.7 V) compatible with a conventional rechargeable Lithium-ion battery. Such an improvement is crucial in enabling consistent and straightforward integration through a battery to various energy harvesters to realize a self-sustainable gas sensor node. Two different 3D-array-based nanogap sensors were fabricated, holding dimensions of 16×16×2 and 25×25×2. The fabricated 3D-nanogap sensors showed (1) that the operational voltages were reduced by 50% from 5V to 2.7 V in comparison to the 2D counterpart and (2) that it successfully detected a VOC (volatile organic compound) of hexanal at a power consumption of only 4 nW.

KEYWORDS

3d nanogap array, Percolation, VOC sensor, Near-zero power sensor.

INTRODUCTION

Despite the recent rise in demands for real-time, battery-free gas monitoring systems for environments, such as industrial regulatory gases of NO_2, SO_2, and CO; agricultural components of NH_3 and VOCs; and oceanic life cycle gases of CO_2, CH_4, and O_2 monitoring [1], a standalone and long-lasting sensor-module has been missing mainly due to the mismatch between power consumption by a gas sensor and power generation by an energy harvester. Power consumption of conventional gas sensors reaches more than 1 mW up to 500 mW [2] due to required heating, focused lights, mechanical vibration, or vacuum [3–5] to achieve the desired selectivity or sensitivity in gas sensing. On the other hand, power generation by an energy harvester, generally depending on the volume, remains at an average level of 0.1 mW/cm^3 or <1 mW for a tiny sensor node of 1's cm^3.

One way of resolving the mismatch in power is to develop an ultra-low-power gas sensor that consumes sub-10-nW power, similar to the leakage power level of recent electronics[6]. Recently, our group has demonstrated a "wake-up" gas sensor that sleeps typically and does not consume any power, resulting in <10 nW power consumption [7–9]. The wake-up gas sensor consisted of a single nanogap (~5 nm) that could capture target gas molecules to form an electrically conductive path during gas detection [8-10]. It was further expanded into a 2D array to enhance reliability in gas detection [11].

However, the recently developed 2D array structure required a higher voltage level of >5 V than the typical output value of a rechargeable battery, additionally requiring a booster circuit and the corresponding power consumption. As a result, the developed 2D nanogap-array-based gas sensor could not be integrated with a mainstream single-cell lithium-ion battery (3.7 V) into a self-sustaining gas sensor node.

To address the high voltage issue while maintaining the sub-10-nW power operation, one can provide a 3D configuration where multiple parallel pathways for electrical conduction exist to lower the overall required voltage.

This paper presents the design, fabrication, and preliminary testing results of a 3D nanogap-array-based gas sensor that achieved both sub-10-nW power consumption and a sub-3.7 V operation voltage.

OPERATION PRINCIPLE

The developed 3D-nanogap array sensor wakes up when captured gas molecules connect one or more random paths for electrical conduction between two electrodes, as shown in Fig.1. Statistically, it is proven that the two electrodes can be connected only when the number of captured gas molecules exceeds a particular threshold value [12]. These captured gas molecules can form bridges in both horizontal and vertical directions, allowing 3D electrical conducting paths. When a complete path is created between the two electrodes, the electrical current flows from one electrode to the other electrode, eventually waking up the rest of the electronics. Thus, this structure remains dormant in the absence of the target particle and starts consuming power only when the target is present.

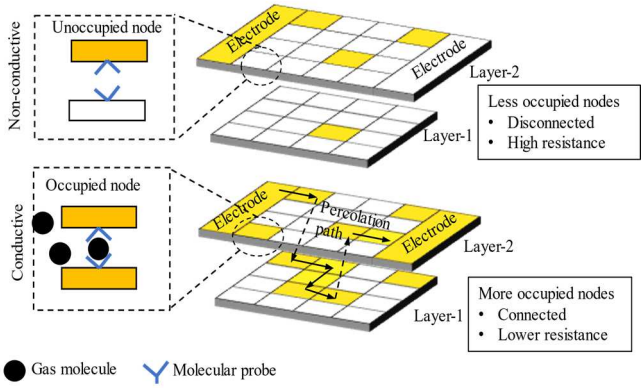

Figure 1: (Left) Single nanogap(5nm) operation: A single nanogap, initially off (top), turns on (bottom) once it captures a target gas molecule with the help of molecular probes. (Right) 3D array operation: A 3D array, initially off (top), turn on (bottom) once it captures a sufficient number

of target gas molecules and forms a continuous path (Percolation path) throughout the 3D configuration.

DEVICE STRUCTURE

The developed 3D array-based gas sensors included two distinctive designs of 16×16×2 and 25×25×2, as illustrated in Fig.2-(a). The array structure mainly consisted of the periodic arrangement of a unit cell of a 2×2×2 structure, as shown in Fig.2-(b). The array structure was formed by stacking three gold layers with an average thickness of 200 nm (Fig.2-(c)). Each gold layer consisted of an array of square-shaped (200×200 μm^2) micro islands, as shown in Fig.2-(d). Between adjacent micro islands, a thin layer of SiO_2 (~4.0nm) and chromium (1~1.3 nm) was deposited and later etched away to produce nanogaps. The SiO_2 layer acted as dielectric insulation, and the Cr layer served as an adhesion layer for the upper gold electrode. After the sacrificial layers (SiO_2 and Cr) were etched, the nanogaps were manifested on the edge at the intersection of micro-islands at different heights, as shown in Fig.2-(e).

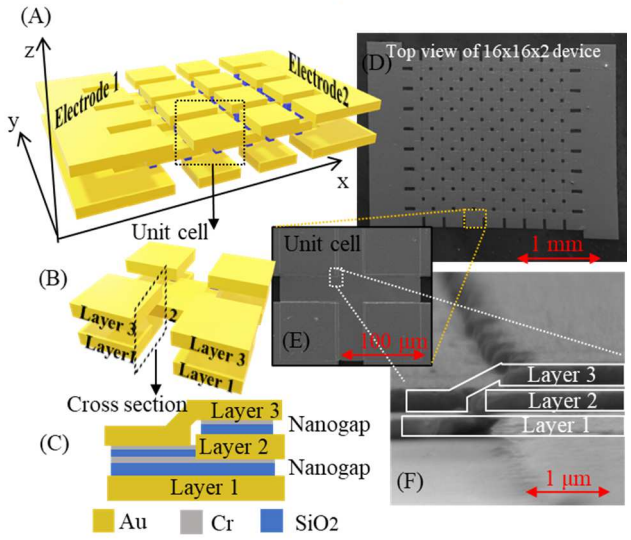

Figure 2: (A) 3D structure gas sensor, (B) A unit cell of the lattice structure, (C) Cross-sectional view double layered nanogap cell (D); Top view of (SEM) 16×16×2 device, (F) Top view of (SEM) a unit cell, and (G) Side view (SEM) of a corner of unit cell indicating the formation of the double layer.

FABRICATION PROCESS

The structure was formed by stacking each layer with sacrificial layers. First, ~500 nm of SiO_2 layer was deposited on a 4-inch Si wafer in the furnace at 1050°C, which provided electrical and thermal isolation of the features from the substrate. The first layer of gold was then sputtered with a chromium layer (~25 nm thickness) for adhesion. The gold layer was patterned using wet lithography to form first layer micro islands of ~200 nm thickness. For lithography, S1813 was used as a photoresist, and AZ300 MIF was applied as the developer. Gold wet etchant was used from Trasene. The gold etches rate was 3 nm/second.

A 4-nm thick coating of SiO_2 was deposited on these micro islands by atomic layer deposition (ALD). 3DMAS (tris(dimethylamine)silane) was used as a SiO_2 deposition precursor in ALD. Then again, the second layer of gold micro-islands was formed with a 1.2-nm Cr layer for adhesion (15 watts of power sputtering). Due to its shallow thickness Cr. layer was sputtered with low power to ensure uniformity of deposition throughout the wafer. The third layer of gold square-shaped micro-islands were formed using a similar process. After completing all deposition processes, the ultra-thin Cr layer was wet etched using diluted (1:10) Cr-etchant. SiO_2 was then etched by RIE (Reactive Ion Etching) to release the nanogaps from the borders of the overlapping micro-islands. For the RIE process, SF_6 gas was used. For the fabrication of a single-layer nanogap sensor (2D percolation based), only two layers of gold electrodes were deposited, and then SiO_2/Cr layer was sandwiched between the two gold layers.

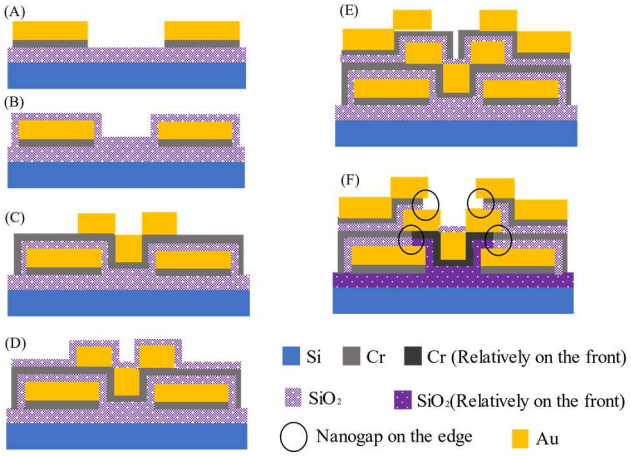

Figure 3: (A) Sputter of layer 1: Cr (25 nm)/Au (200 nm), (B) ALD of sacrificial layer (SL): SiO_2 (4 nm), (C) Sputter of layer 2: Cr (1.2 nm)/Au (200 nm), (D) ALD of SL: SiO_2 (4 nm), (E) Sputter of layer2: Cr (1.2 nm)/Au (200 nm), (F) Recurring wet and dry etch (RIE) to form nanogaps.

TESTING METHODOLOGY

Sensor preparation for testing

Fabricated sensors were first coated with molecular probes for functionalizing the gold electrodes of nanogap. The production process of these molecular probes (linkers) was discussed in a previous publication [10]. The fabricated sensor structures were immersed in the linker solution for 36 hours to functionalize the fabricated sensors and then cleaned with a DMF (Dimethylformamide) solution and acetone for 5 min and 2 min, respectively.

Gas exposure

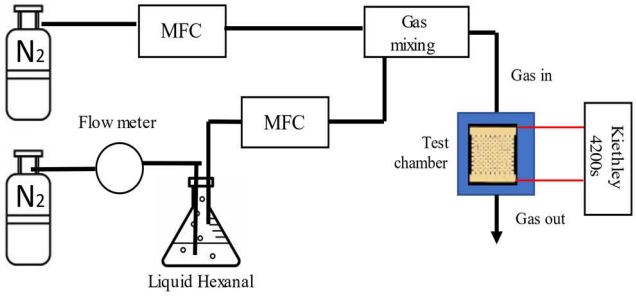

Figure 4: Flow-based hexanal gas (VOC) measurement set-up for hexanal sensing.

Figure 4 shows the testing set-up to verify the responses of the fabricated sensor to various concentrations of commercial Hexanal (Sigma Aldrich). The fabricated nanogap-array-based sensor was placed in a microprobe station (MPS) testing chamber (Nextron). The inlet of the testing chamber was connected to a gas mixing chamber where the dilution of pure hexanal vapors occurred by mixing with nitrogen gas. The hexanal vapor was generated by controlling the flow of N_2 in a liquid hexanal-containing flask. The flask was shielded; thus, N_2 flow generated bubbles inside the liquid hexanal. The produced bubbles were carried into a mixing chamber by a mass flow controller (MFC). Concentrations of hexanal were controlled from 43.20 ppm to 1081.34 ppm.

The following formula calculated the concentration of the target gas:

$$C\ (ppm)=\frac{\frac{P\times L}{760-L'}}{\frac{P\times L}{760-L}+L+L'}\times 10^6$$

where L and L′ were the gas flow rates of N_2 (through the bubbler) and air, respectively; P was the vapor pressure of Hexanal (in mm of Hg) at room temperature. After each testing, the chamber was purged with N_2 for ~2 hours.

Electrical Measurement and characterization

The two electrodes of the 3D-nano-gap-array sensor were probed with Keithley 4200S. Firstly, the I-V graph of each device was monitored by applying incremental voltage and measuring the current for each voltage. By observing the I-V characteristics graph, a bias voltage was chosen that allows the sensor to run at its highest sensitivity. Secondly, the selected bias voltage was applied to the sensor while the device's resistance was monitored continuously during the exposure and purging of Hexanal gas.

RESULT AND DISCUSSION

I-V Characteristics

Measurement results clearly showed that the sensor structure successfully formed the metal-insulator-metal (MIM) junctions that were governed by quantum properties, showing both Direct Tunneling (DT) and Fowler-Nordheim Tunneling (FNT), as shown in Fig.5.

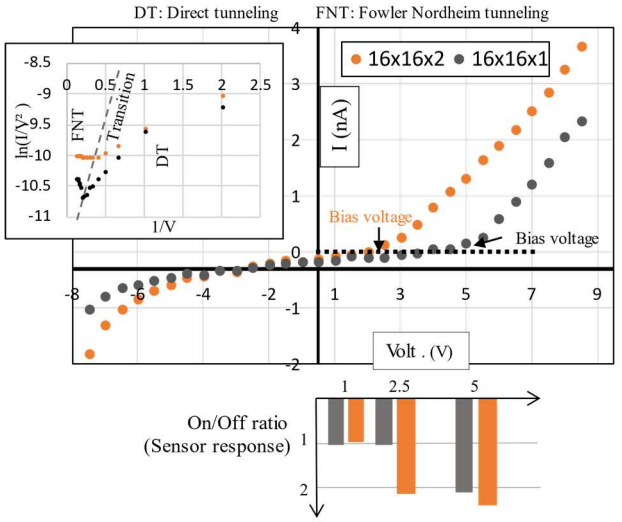

Figure 5: I-V curve of a 16×16×2 structured device. (Top left) I-V curve indicated a bias voltage for DT to FNT transition, which was further verified by the tunneling current graph. (Bottom)Below the bias voltage, the sensor response is very trivial; on the contrary, above the bias voltage sensor response remains almost similar

Note that DT and FNT can be defined as below[11]:

$$I_D \propto V \exp\left[\frac{-4\pi d\sqrt{2\phi m^*}}{\hbar}\right]\text{.....(i)}$$

$$I_{FN} \propto V^2 \exp\left[\frac{-8\pi d\sqrt{2\phi^3 m^*}}{3q\hbar V}\right]\text{.....(ii)}$$

Here, I_{FN} and I_D is current during direct tunneling and Fowler–Nordheim tunneling, respectively. Where ϕ is the barrier height, m* is the effective mass of electrons, V is the applied voltage, and d is the thickness of the dielectric layer. It was observed that in the FNT region, the change of current was proportional to the cube of $\sqrt{\phi}$, whereas in DT region, the current was proportional to $\sqrt{\phi}$. Thus, in the FNT region, the device was more responsive, as shown in Fig.5-bottom. However, if a MIM junction was kept deep in the FNT region for ample time, dielectric breakdown happened to cause permanent damage to the MIM junction. Thus, a bias voltage was chosen in such a way that sensor response was maximized while dielectric breakdown was prevented.

Bias voltage reduction in multi-level structure

In the fabricated multi-level structure (a 3D nanogap array), the required bias voltage was reduced by 50% compared to a 2D structure. The voltage reduction was mainly due to parallel conducting paths across two layers. Figure 6A shows the top view of 16×16×2 and 25×25×2 devices. Figure 6B compares the bias voltages in different designed structures.

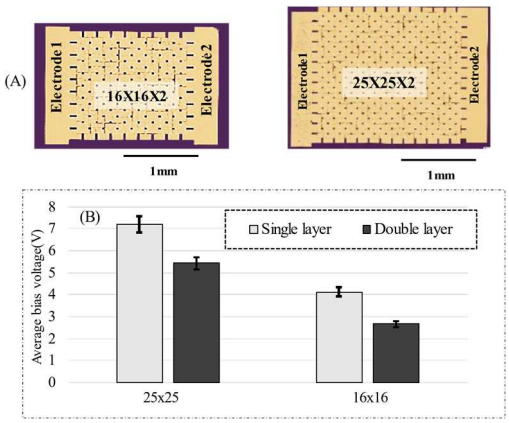

Figure 6: (A)Top view of 16×16×2 and 25×25×2 array. (B)The bias voltage was reduced by almost 50% in double-layered structures. For 16×16 and 25×25 structure, bias voltage is <3.8V, Thus, these double layer structures are single-cell rechargeable battery integrable without the use of any boost converter.

Gas sensing operation

With the exposure of 100 ppm Hexanal VOC gas, the response of the sensor was measured 2.38 times. The response was recorded for 3 continuous exposure and purging. The sensor response was defined as the following formula:

$$\text{Response (On/Off ratio)} = \frac{\text{Resistance at the presenece to gas}}{\text{Resistance at the absence of gas}}$$

When the sensor was continuously purged and exposed to Hexanal VOC, it showed similar repetitive

responses, as shown in Fig.7. The power consumption of the sensor was calculated as only 1.3 nW during the absence of target gas molecules and 3.27 nW during the presence or detection of the target gas particles. After the exposure of Hexanal VOC particles, it took nearly 500 seconds to lower the resistance to a stable saturated value; during purging, it took almost 100 seconds to return to the initial value. This behavior was almost identical when exposed to 100 ppm Hexanal gas.

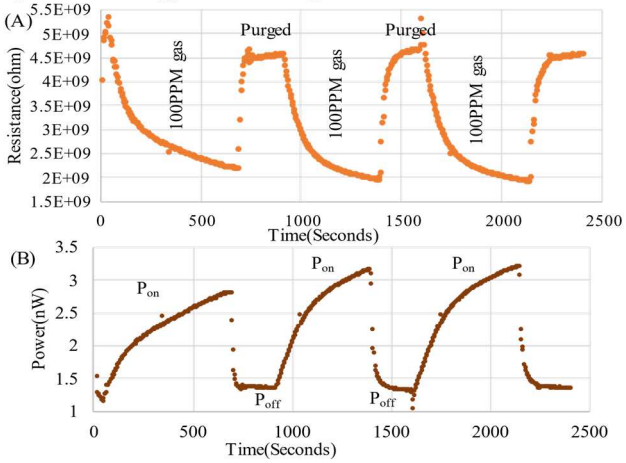

Figure 7: (A) Repeated response of a 16×16×2 sensor with 100ppm gas exposure and purge. (B) Corresponding power consumption by the sensor.

A comparison between the single layer (2D structure) and double layer (3D structure) is shown in the table below.

Table 1: Comparison between 2D and 3D structure

	Single Layer (16×16×1, 25×25×1)	Double Layer (16×16×2, 25×25×2)
Bias voltage	>5 V	>2.7 V
Power requirement	<1 nW	1~4 nW
Quantum tunneling probability	Comparatively lower	Comparatively higher
3.7 V rechargeable battery connectable	No	Yes

CONCLUSION

We have successfully demonstrated the design, fabrication, and testing results of the 3D nanogap array-based Hexanal VOC sensor. Two different 3D structures (16×16×2 and 25×25×2) were fabricated. Two comparable 2D structures (16×16×1 and 25×25×1) were also fabricated for comparison. In the double-layer structure, quantum tunneling probability was doubled that of the single-layer structure, as evidenced by the reduced operating voltage. Thus, the bias voltage was lowered to <3.7 V in the microfabricated 3D structure, which becomes compatible with a single-cell rechargeable battery without additional circuitry. This research indicated the feasibility of an ultra-low-power sensor with a low operation voltage that can be directly connected to various energy harvesters to enable a self-sustaining sensor node.

ACKNOWLEDGMENT

The information, data, or work presented herein was generously supported by the Advanced Research Projects Agency-Energy (ARPA-E) OPEN 2018 program (PM: Dr. David Babson) under the award number of DE-AR0001064 and by the Defense Advanced Research Projects Agency (DARPA) NZERO Program (PM: Drs. Benjamin Griffin and Troy Olsson) under the cooperative agreement of HR0011-15-2-0049. The microfabrication was performed in the state-of-the-art Utah Nanofabrication Facility (Director: Prof. Hanseup Kim) in the University of Utah.

References

[1]. S. Dhall, B. R. Mehta, A. K. Tyagi, and K. Sood, "A review on environmental gas sensors: Materials and technologies," Sensors International, vol. 2, p. 100116, 2021.

[2]. A. Baranov, D. Spirjakin, S. Akbari, and A. Somov, "Optimization of power consumption for gas sensor nodes: A survey," Sens Actuators A Phys, vol. 233, pp. 279–289, Sep. 2016.

[3]. S. Feng et al., "Review on Smart Gas Sensing Technology," Sensors, vol. 19, no. 17, p. 3760, Aug. 2019.

[4]. F. Xu and H.-P. HO, "Light-Activated Metal Oxide Gas Sensors: A Review," Micromachines (Basel), vol. 8, no. 11, p. 333, Nov. 2017.

[5]. A. Dey, "Semiconductor metal oxide gas sensors: A review," Materials Science and Engineering: B, vol. 229, pp. 206–217, Mar. 2018.

[6]. N. Yu, Y. Miao, L. Mu, H. Du, H. Huang, and X. Jia, "Minimizing Energy Cost by Dynamic Switching ON/OFF Base Stations in Cellular Networks," IEEE Trans Wirel Commun, vol. 15, no. 11, pp. 7457–7469, Nov. 2016.

[7]. S. H. Khan et al., "Characterization of a Wake-Up Nano-Gap Gas Sensor for Ultra Low Power Operation," Journal of Microelectromechanical Systems, vol. 31, no. 5, pp. 791–801, Oct. 2022.

[8]. S. K. M. Truong et al., "Demonstration of 155.1 µW Wake-Up Gas Sensor Node Toward 8 Month Lifetime," in 2020 IEEE 33rd International Conference on Micro Electromechanical Systems (MEMS), Jan. 2020, pp. 622–625.

[9]. A. Banerjee et al., "Molecular bridge-mediated ultralow-power gas sensing," Microsyst Nanoeng, vol. 7, no. 1, p. 27, Dec. 2021.

[10]. S. H. Khan et al., "Development of a Gas Sensor for Green Leaf Volatile Detection," in 2021 21st International Conference on Solid-State Sensors, Actuators and Microsystems (Transducers), pp. 250–253 Jun. 2021.

[11]. F. Ahmed, M. S. Choi, X. Liu, and W. J. Yoo, "Carrier transport at the metal–MoS 2 interface," Nanoscale, vol. 7, no. 20, pp. 9222–9228, 2015.

CONTACT

* Farhan Sadik Sium,
Tel: +1-385-867-3783; Email: farhan.sium@utah.edu